RSC Advances

PAPER

View Article Online
View Journal | View Issue

Cite this: *RSC Adv.*, 2014, **4**, 23886

Energy and environmental usage of super porous poly(2-acrylamido-2-methyl-1-propan sulfonic acid) cryogel support

Nurettin Sahiner*[ab] and Fahriye Seven[b]

Superporous and nonporous poly(2-acrylamido-2-methyl-1-propansulfonic acid) [p(AMPS)] cryogels and hydrogels were prepared under freezing conditions (−18 °C) and at room temperature (25 °C), respectively. The swelling equilibrium values of the p(AMPS) cryogels were extremely fast, 3600 fold faster than those of conventional hydrogels. The p(AMPS) cryogels were further employed as highly effective supports for the *in situ* preparation of metal nanoparticles within superporous networks, by loading Co(II) and Ni(II) ions into the cryogel network from aqueous environments and reducing with $NaBH_4$. The Co metal nanoparticle-containing cryogel composites demonstrated superior catalytic performances in comparison to nonporous p(AMPS) hydrogel composites for energy and environmental applications *e.g.*, hydrogen production from the hydrolysis of sodium borohydride, and reduction of 4-nitrophenol to 4-aminophenol. The energy applications of cryogel-based p(AMPS)–Co metal composites, especially, were investigated in detail. The effect of various parameters on the rate of the hydrogen generation reaction, such as porosity, metal types, pH, the types of reaction water, temperature and reuse of catalyst, were examined for the p(AMPS)–Co cryogel composite materials. With the p(AMPS)–Co cryogel composite a very high hydrogen generation rate of 14 501 mL H_2 per min per g of Co was attained. This value is one of the best recorded values in comparison to the values obtained for other similar catalysts reported in the literature. p(AMPS)–Co composite cryogels were repeatedly used without significant loss of catalytic activity (82%) even after five repetitive uses for catalytic hydrolysis reactions with $NaBH_4$. Additionally, a very low activation energy for the p(AMPS)–Co cryogel composite systems was attained: $E_a = 15.40 \pm 0.3$ kJ mol^{-1}.

Received 17th February 2014
Accepted 14th April 2014

DOI: 10.1039/c4ra01386g

www.rsc.org/advances

1. Introduction

In recent years, innovative research has been carried out with regard to energy and environmental concerns.[1,2] Energy is essential to maintain all activities in daily life. However, the production, transportation and use of energy, which is obtained principally from fossil fuels, is the root of major adverse effects on the environment and on health. Therefore, the generation of renewable, clean and inexhaustible energy is of crucial significance.[3,4] Many researchers have focused on hydrogen energy as it is renewable, clean, safe, cheap and easily generated from the hydrolysis of various storage materials such as chemical hydrides.[5,6] In addition to drawbacks in energy production, the major concern for the environment and human health is the existence of hazardous organic toxic chemicals. Amongst the organic pollutants, halogenated organic compounds and their derivative nitrophenols (4-NP) are a major concern because of their high toxicity, carcinogenic nature, and low biodegradability, they accumulate in waste water as they are used in many industries such as the production of anilines, paper, explosives, pharmaceuticals, dyes, and therefore cause many problems.[7,8] Due to its favorable properties such as having a selective strong reducing capability, being a hydrogen generator and storage material, and its usefulness in manufacturing pharmaceuticals, and fine chemicals, $NaBH_4$ is a preferred material attracting great attention over the past decade and is one of the mostly frequently used materials for various applications, as stated earlier.[9–11] $NaBH_4$ can be used for hydrogen generation from the hydrolysis reaction in the presence of a catalyst, and for the reduction of toxic nitrophenols and their derivatives to environmentally friendly amino phenols.[12,13] In the use of metal nanoparticles as catalysts, aggregation problems, and the stabilization of metal nanoparticles (generally ~5–100 nm) to prevent early oxidation and poisoning, are the most cumbersome problems and can be overcome by employing nanotechnology and polymer science.[14,15] Recently, we have reported the use of a smart hydrogel as a template for the preparation of metal nanoparticles taking advantage of their hydrophilic 3-D

[a]*Canakkale Onsekiz Mart University, Faculty of Sciences and Arts, Chemistry Department, 17100, Canakkale, Turkey. E-mail: sahiner71@gmail.com; Fax: +90-2862181948; Tel: +90-2862180018-2041*

[b]*Nanoscience and Technology Research and Application Center (NANORAC), Terzioglu Campus, 17100, Canakkale, Turkey*

networks which have different numbers of functionalities including –OH, –COOH, $–NH_2$, $–CONH_2$, and $–SO_3H$ and are able to bind easily to metals without dissolving in aqueous media They provide a range of environmentally responsive behaviors, such as bending, degrading, swelling, shrinking, and color changing against environmental factors such as pH, solvent, temperature, electric field, magnetic field, *etc.*[16–18] Despite the advantages of common hydrogels, the diffusion of solvents, metal ions or any reactant into the hydrogel network remains the foremost tiresome and time consuming problems for the *in situ* preparation of nanoparticles within a hydrogel network or for their use as reactants in catalytic applications. To improve their responsive properties, nano-, micro- and macropores can be generated within hydrogel networks by various techniques. One alternative solution is to use hydrogel networks with macro- or superpores (of the order of a few tens of micrometers) that can be generated within hydrogels by preparing them under cryogenic conditions, namely as cryogels. Recently much progress has been made in the cryogelation method by preparing hydrogels under cryogenic conditions.[19–22] The cryogelation method includes the use of a large amount of pure water, nearly 90–95 wt% of the initial solution. The polymerization and crosslinking reaction can be carried out around frozen water molecules (ice-crystals) under freezing conditions. During the polymerization reaction, most of the water molecules are converted to ice crystals, whereas bound water and other solutes in the reaction medium, such as the initiator, crosslinking agent, catalyst and monomer molecules, accumulate in a non-frozen liquid microphase.[23–25] Cryogenic network formation progresses *via* polymerization of the non-frozen liquid microphase around the ice-crystals that act as a porogen. Upon thawing the ice-crystals within the gel matrix, a superporous cryogel is formed that has large pores with variable size and geometry depending on the shape of the ice-crystals.[26,27] Furthermore, the natural characteristics of the cryogels, such as the super pore size, pore wall thickness, elasticity, and mechanical strength, can be tuned by adjusting the preparation conditions, and the composition of the solutions, such as the amount of water or organic co-solvents, cooling rate, temperature gradient, solute concentrations, precursor composition, *etc.* Interconnected macropores within the three-dimensional cryogenic networks enable the retention and release of water or any solvent which is absorbed within the large pores by a diffusion pathway *via* reversible squeeze–relaxation cycles under definite pressure.[28–31] Due to their discernible properties, most notably their fast responsiveness, structural flexibility, high mechanical resistance, large pores, and fast diffusion pathways, cryogels can respond to external stimuli such as pH, solvent, and ionic strength *etc.* much faster than conventional hydrogels.[32,33] Moreover, these properties of cryogels make them ideal fast metal ion binding materials, and catalyst supports for *in situ* metal nanoparticle preparation.[16–18] Cryogels containing metal composites can be used as catalysts for H_2 generation for energy applications, and for the reduction of nitro compounds for environmental applications.

Therefore, we report the use of poly(2-acrylamido-2-methyl-1-propansulfonic acid) [p(AMPS)] cryogels and hydrogels prepared by a free radical polymerization technique at freezing and room temperatures, and used them for *in situ* metal nanoparticle preparation by loading Co and Ni ions from their aqueous solutions and reduction. Finally, we also demonstrated the use of p(AMPS)–M (M: Co, Ni) cryogel composites for H_2 generation *via* $NaBH_4$, and in an environmental application for the reduction of 4-NP to 4-AP. Various parameters affecting the H_2 generation performance were evaluated and compared with the literature.

2. Materials and methods

2.1. Materials

The monomer, 2-acrylamido-2-methyl-1-propanesulfonic acid (AMPS, 50 wt%, Sigma-Aldrich), the crosslinker, *N*,*N*′-methylenebisacrylamide (MBA, 99%, Across), the initiators, ammonium persulfate (APS, 99%, Sigma-Aldrich) or potassium persulfate (KPS, 99%, Sigma-Aldrich), and the accelerator, *N*,*N*,*N*′,*N*′-tetramethylethylene diamine (TEMED, 98%, Across) were used as received for the hydrogel and cryogel preparation. Cobalt(II) chloride hexahydrate ($CoCl_2 \cdot 6H_2O$, 99%, Sigma-Aldrich) and nickel(II) chloride hexahydrate ($NiCl_2 \cdot 6H_2O$, 98%, Sigma-Aldrich) were used as metal ion sources for nanoparticle preparation. Sodium borohydride ($NaBH_4$, 98%, Merck) was used as the reducing agent and as the H_2 source in the hydrolysis reaction. 4-Nitrophenol (4-NP, 99%, Merck) was used as the organic compound in the catalytic reduction reaction. Sodium hydroxide (NaOH, 97%, Sigma-Aldrich), and hydrochloric acid (HCl, 37%, Sigma-Aldrich) were used for the preparation of acidic and basic solutions. Tap water, water from Sarı Çay creek, and sea water were used as the reaction media for the same hydrogen generation reactions. Distilled (DI) water of 18.3 MΩ cm^{-1} was used for the experimental studies.

2.2. Synthesis of p(AMPS) hydrogels and cryogels

Synthesis of p(AMPS) hydrogel was carried out *via* a free radical polymerization technique. Briefly, 5 mL of AMPS, 0.002 g of MBA (0.1% mole ratio of monomer) and 5 μL of TEMED were mixed to obtain an homogenous solution, and 1 mL of APS initiator solution (1% mole ratio of monomer) was added by mixing. The obtained hydrogel precursor was placed in plastic straws of about 0.4 mm diameter. The reaction was completed within 15 min and the obtained cylindrical hydrogels were cut to 2–3 mm in length, and washed with DI water for 12 h by placing in excess amounts of water and replacing the water every 3 h.

The preparation of p(AMPS) cryogel was performed *via* a cryopolymerization technique. An ice bath was used to cool the AMPS precursors before cryopolymerization. Firstly, 0.78 mL of AMPS aqueous solution (50 wt%) was added to 6.22 mL of DI water in order to obtain a monomer ratio of 6 w/v% within the total solution volume of 8 mL. Then, 0.0354 g of MBA (10% mole ratio of monomer), and 50 μL of TEMED were added into the monomer solution and mixed by using a vortex mixer. Separately, 0.0054 g of KPS (1% mole ratio of monomer) was dissolved in 1 mL of DI water, and cooled under constant mixing in

an ice-bath for 5 min. Finally, this redox initiator solution was added to the cooled monomer mix, and then this mix was placed in plastic straws (about 8 mm in diameter). The cryogelation was achieved in a deep freezer at −18 °C for 24 h *via* free-radical crosslinking polymerization. Finally, the obtained cryogels were thawed at room temperature, and cut into smaller dimensions of 2–3 mm. The acquired cryogels were cleaned by washing with plenty of DI water to remove the unreacted species such as the monomer, polymer, crosslinker and initiator from the cryogenic matrices. The obtained cryogels were dried in an oven at 45 °C for further experimental studies.

2.3. Synthesis of metal nanoparticles within conventional hydrogel and superporous p(AMPS) cryogel matrices

The preparation of metal nanoparticles inside the network structure was carried out by metal loading from aqueous solutions and *in situ* reduction. Briefly, 100 mg of dried hydrogel and cryogel samples were placed in 100 mL of 500 ppm M(II) (M = Co or Ni) solutions at a constant mixing rate of 500 rpm, at room temperature, for 24 h. Then, to remove the unattached metal ions from the polymeric networks, metal ion-loaded polymeric networks were washed with distilled water for 30 min. After washing, the metal ion-loaded hydrogels and cryogels were placed in 50 mL of 0.2 M $NaBH_4$ solution for 3 h at a stirring rate of 500 rpm at room temperature for the reduction of metal ions *in situ* within the polymeric networks to their corresponding metal nanoparticles. Finally, the hydrogel or cryogel-M composites were washed with DI water again, and used for catalytic applications.

3. Results and discussion

3.1. Characterization of nonporous, superporous polymeric networks and their metal-containing composites

The swelling characteristics, pore sizes and pore structures of conventional hydrogel and novel cryogel networks were determined through swelling experiments, optical microscopy (Olympus bX53) and scanning electron microscopy (SEM, JEOL

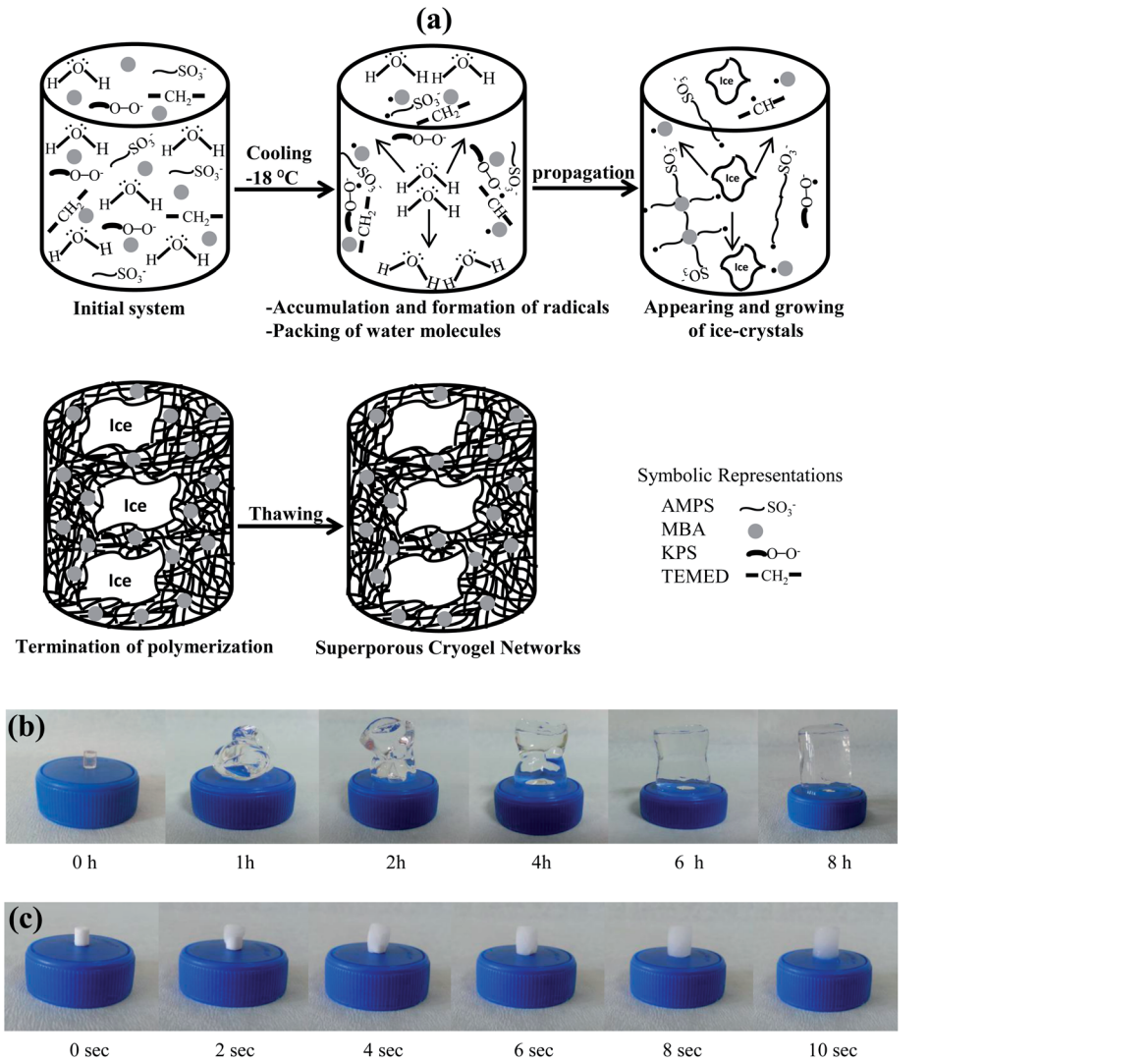

Fig. 1 The polymerization mechanism of p(AMPS) cryogels (a), and visual demonstration of the swelling of 0.1% crosslinked p(AMPS) hydrogels (b), and (c) 10% crosslinked p(AMPS) cryogels.

2010) analysis. The metal ion absorption capacity and the metal nanoparticle contents of the hydrogel and macroporous cryogels were determined by atomic absorption spectroscopy (AAS, Thermo ICA 3500 AA SPECTRO) measurements. The size of the metal particles inside the bulk cryogel matrices was determined *via* transmission electron microscopy (TEM, JEOL 2010) analysis. Finally, the thermal behaviour of the hydrogels, cryogels and their various metal composites were investigated by thermogravimetric analysis (TGA/DTA-SII 6300).

To visualize the mechanism of cryopolymerization, a representation of the cryopolymerization reaction of the non-frozen liquid microphase occurring around the growing ice-crystals is illustrated in Fig. 1(a). Firstly, the initiator activated by the catalyst and the generated radicals reacts with the monomer and crosslinker to produce branched oligomers and macromers *etc.*, followed by polymerization and the crosslinking reaction around the ice-crystals, thus a frozen cryogel network is obtained. Upon completion of polymerization and the crosslinking reaction, and after thawing, macrometer sized pores are formed within the 3-D polymeric matrices in place of the ice-crystals, as can be seen in the figure.

As the swelling behaviour is one of the most important characteristics of hydrogels, the swelling behaviour of p(AMPS) hydrogels and cryogels was investigated. Swelling studies of hydrogels and cryogels were carried out by means of mass increase by placing the dried and weighed polymeric networks within 100 mL of DI water, removing them at certain time intervals and determining their mass increase with time. The maximum percent swelling (S_{max} %) of the hydrogels and cryogels were calculated as about 28 000% and 500% according to eqn (1) and (2). So, the high swelling degree of 0.1 mole % crosslinked p(AMPS) hydrogel implies that it contains greater amounts of water (~56 fold) than 10% crosslinked p(AMPS) cryogel.

$$\% S = [(m_{\text{wet hydrogel}} - m_{\text{dry hydrogel}})/m_{\text{dry hydrogel}}] \times 100 \quad (1)$$

$$\% S = [(m_{\text{squeezed cryogel}} - m_{\text{dry cryogel}})/m_{\text{dry cryogel}}] \times 100 \quad (2)$$

As illustrated in Fig. 1(b) and (c), the time to reach S_{max} % for hydrogels and cryogels is quite different with the hydrogels reaching their S_{max} % at about 8 h, and the cryogels reaching S_{max} % within 10 s. It is obvious that the swelling time for the superporous cryogel is almost 3600 times shorter than the corresponding conventional hydrogel, even though it has 100 fold more crosslinks with a lower swelling ratio. In fact, this behaviour is due to differences in their preparation methods. As cryogels have a high degree of crosslinker with a very large interconnected porous structure and a low specific surface area compared to their counterpart hydrogels, they swell quickly, within seconds, with a small amount of water uptake in comparison to normal hydrogels.[34,35] The fast swelling property of cryogels provides many advantages. For example, the main advantages of the higher swelling rates, and faster swelling of cryogels provide fast process times in cleaning of cryogels, and loading of cryogels with different species such as metal ions and their reduction to corresponding metal nanoparticles, and eventually result in faster catalytic performance in their catalytic applications.

Furthermore, the % porosity of cryogels was roughly calculated as 78.60% according to the following equation:

$$\% \text{ Porosity} = [(m_{\text{wet cryogel}} - m_{\text{squeezed cryogel}})/m_{\text{wet cryogel}}] \times 100 \quad (3)$$

The interconnected and highly open structures of p(AMPS) cryogels were examined through SEM analysis, and the optical microscope images are illustrated in Fig. 2(a) through (f). The pore structures of dried p(AMPS) cryogel samples were obtained as a thin film using a freeze-dryer under a vacuum. As can be seen in Fig. 2(a)–(f), the pore size of the cryogels was more than 50 μm. Highly interconnected and open pores of cryogels provide a faster contact time with the metal nanoparticles embedded within them with reactants in the reaction medium. It is obvious that the highly porous network and fast responsive nature of cryogels make them indispensable materials in the design of advanced template materials *e.g.*, for metal nanoparticle preparation and for use as catalyst systems for catalytic applications. Here, we prepared Co and Ni metal nanoparticles as catalyst systems by using $NaBH_4$ as the reducing agent within p(AMPS) cryogels *via* an *in situ* reduction method. For that purpose, Co(II) or Ni(II) metal ion-loaded 0.1 g p(AMPS) cryogels were treated with 50 mL of 0.2 M $NaBH_4$ solution at a mixing rate of 500 rpm for 3 h. As clearly demonstrated in Fig. 3(a), Co(II) ions inside the cryogel matrices were converted to Co metal nanoparticles by $NaBH_4$ treatment. Furthermore, the TEM images of p(AMPS)–Co composites show that the size of the Co metal particles are nanoscale, ranging from about few

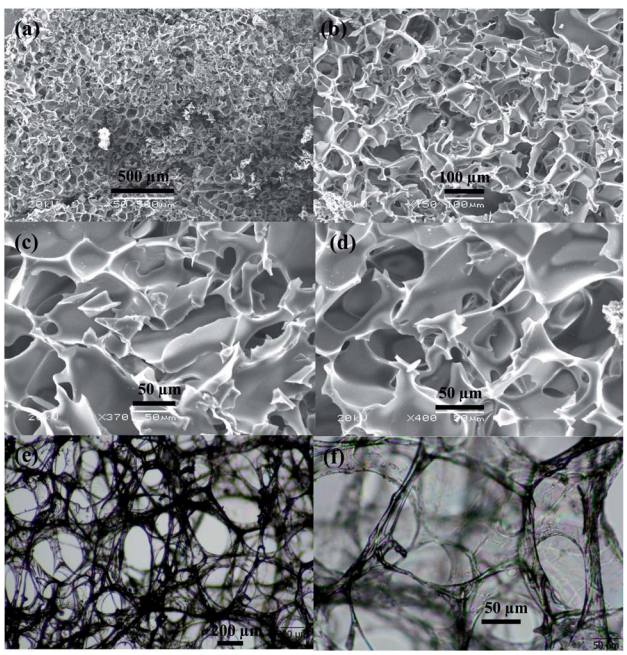

Fig. 2 SEM images of p(AMPS) cryogels under (a) 50, (b) 150, (c) 370, and (d) 400 magnification, and optical microscope images of p(AMPS) cryogels under (e) 10× and (f) 20× magnifications.

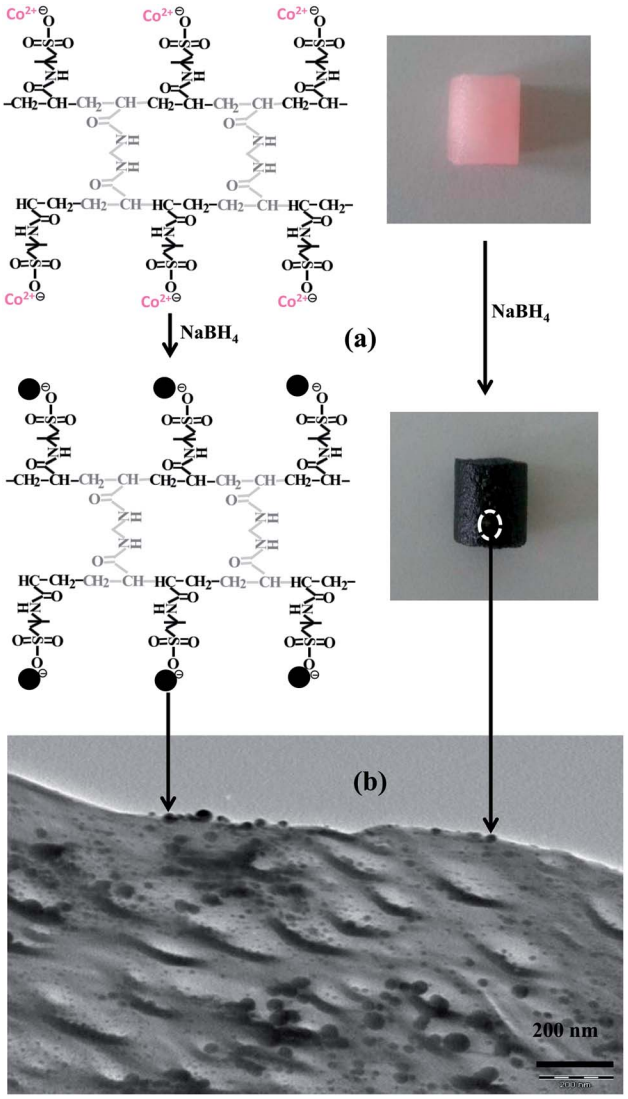

Fig. 3 (a) The reduction of Co(II) ions to cobalt nanoparticles within cryogel matrices, and (b) TEM images of cobalt nanoparticles within porous cryogel networks.

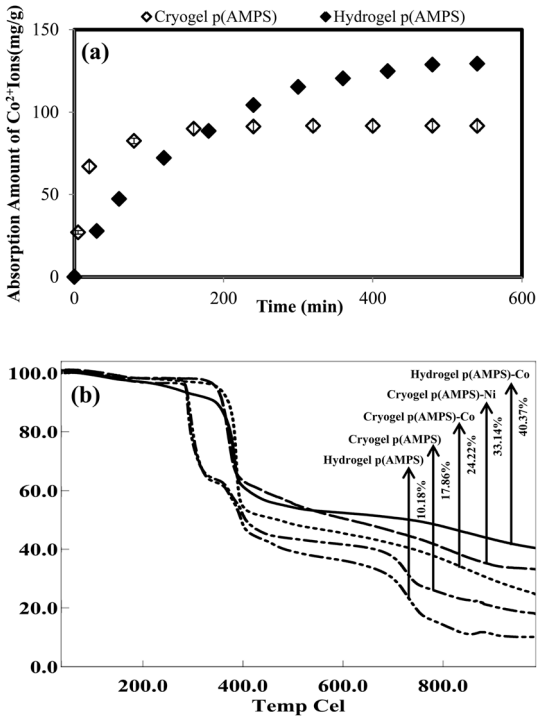

Fig. 4 (a) Metal ion absorption capacities of p(AMPS) hydrogels and cryogels, and (b) TGA thermogram of p(AMPS) hydrogel, cryogel and their metal nanoparticle-containing composites.

tens of nm to about 50 nm as seen in Fig. 3(b). The TEM images were obtained by grinding samples of p(AMPS)–Co composite suspension in acetone and a few drops of these composites were placed on carbon coated Cu TEM grids. The TEM images were then acquired under an electron beam, accelerated by an applied 200 kV in vacuum. As demonstrated in TEM images, the Co particles are almost homogeneously distributed throughout the p(AMPS) cryogel matrices.

The fast responsive behavior of porous p(AMPS) cryogels and the corresponding hydrogels were compared in terms of Co(II) ion absorption times and amount as illustrated in Fig. 4(a). About 1.0 g of p(AMPS) cryogel and hydrogels were immersed in 500 mL of 500 ppm $CoCl_2 \cdot 6H_2O$ solution at a mixing rate of 500 rpm. It was found that 91.70 mg of Co(II) ions were absorbed by the cryogels at the end of 4 h, whereas 129.35 mg Co(II) ions were absorbed by the hydrogels at the end of 8 h. Although the Co(II) ion absorption time of the cryogels is about two fold shorter than that of the hydrogel, the Co(II) ion absorption capacity is much less than that of the hydrogels. This is generally the case for cryogels because the specific surface area is lower for the cryogels of p(AMPS) than that of the corresponding hydrogels. The only downside of cryogels is their lower specific surface area as has been reported in the literature.[34,35] In addition to the comparison of their metal ion absorption capacities, the metal nanoparticle contents were also determined *via* an acid dissolution method in which metal nanoparticle-containing cryogels and hydrogels were treated with concentrated HCl. Thus, 0.1 g of p(AMPS)–M (M: Co or Ni) composites were treated with 50 mL of 5 M HCl solution for 12 h three times repeatedly, and the elution solution was diluted at a ratio of 1/150 with pure water. The amount of metal ions within each polymeric matrix was measured by AAS. The amount of Co nanoparticles within 1 g of cryo-p(AMPS) was found to be 86.27 mg g^{-1}, whereas the amount of Co metal nanoparticles inside 1 g of hydrogel–p(AMPS) was 124.88 mg g^{-1}. As can be seen these values are consistent with their absorbed amounts. The metal contents of the cryogels and hydrogels are given in Table 1. Additionally, the metal content of each polymeric matrix was also confirmed *via* TGA as seen in Fig. 4(a) and Table 1. The thermal behavior of the p(AMPS) cryogels, hydrogels and their metal particle-containing composites were determined *via* TGA by heating about 2 mg of dried samples from 50 to 1000 °C at a heating rate of 10 °C min^{-1} under a nitrogen flow at 100 mL min^{-1}. As can be seen, the thermal behavior of the p(AMPS) cryogels and hydrogels seem very similar whereas their metal nanoparticle-containing composites are different, depending

Table 1 The amount of metal nanoparticles, TGA results, TOF (Turn Over Frequency) values and Hydrogen Generation Rates (HGR) for various catalyst systems[d]

Metal composites	[a]Amount of metal nanoparticles	Weight loss % by TGA (%) at 1000 °C	[b]TOF	[c]HGR
Hydrogel p(AMPS)–Co	124.88 ± 1	40.37	2.24 ± 0.2	950.90 ± 0.3
Cryogel p(AMPS)–Co	86.27 ± 1.2	24.22	6.37 ± 0.1	2697.91 ± 0.5
Cryogel p(AMPS)–Ni	89.41 ± 1.5	33.14	1.64 ± 0.12	699.11 ± 0.2
3rd Loading p(AMPS)–Co	195.42 ± 1	53.11	6.25 ± 0.1	2648.92 ± 0.2
Magnetic p(AMPS)–Co	87.16 ± 1.2	57.45	2.75 ± 0.3	1171.54 ± 0.1

[a] The amount of metal nanoparticles within a cryogel/hydrogel as mg g^{-1} determined by AAS measurements. [b] TOF (Total Turnover Frequencies) [mol H_2 per mol catalyst per min]. [c] HGR (Hydrogen Generation Rate) [mL of H_2 per min per g of M]. [d] Reaction conditions: 50 mL of 50 mM $NaBH_4$, 5% NaOH, 1000 rpm, 30 °C.

on the metal types and their amounts. It can be inferred that the p(AMPS) cryogels and hydrogels start to degrade very sharply at about 300 °C, whereas the onset of sharp degradation of their metal nanoparticle-containing composites occurs at about 350 °C. The p(AMPS) cryogels and hydrogels and their composites have different degradation temperatures as shown in the TGA thermograms and this continues up to 1000 °C as illustrated in Fig. 4(b). The weight losses of the p(AMPS) cryogels and their Co nanoparticle-containing composites were 22.58 and 17.65 wt%, whereas the weight losses of the p(AMPS) hydrogels and their Co composites were 44.45 and 10.18% at 985 °C. Consequently, due to the high crosslinking degree of the cryogels, they have higher thermal stability than conventional hydrogels. On the other hand, due to their low metal nanoparticle content, the composites are less thermally stable than the metal composites of the hydrogels. The thermal resistances of other metal composites are given in Table 1, it can be seen that the metal nanoparticle-embedded p(AMPS) networks, whether hydrogel or cryogel, are thermally more stable and have less sharp degradation temperature ranges than their bare hydrogel or cryogel counterparts. Therefore, it can be concluded from TGA analysis that the p(AMPS) cryogel metal composites can be safely used at temperatures ranging from room temperature up to 200 °C without any significant weight loss. The higher thermal stability of the cryogels could be due to the high amount of crosslinker used for the cryogels than for the hydrogels as the crosslinking degree of the cryogels is approximatelyone-hundred fold higher than those of the hydrogels.

3.2. Energy and environmental applications of p(AMPS)–Co metal composites

To demonstrate the potential use of p(AMPS) hydrogels and cryogels in energy and environmental applications, H_2 generation and reduction of 4-NP were carried out using $NaBH_4$ as the hydrogen source, and as a reducing agent using p(AMPS)–M based materials as catalysts. The reaction mechanisms of both the catalytic reactions are shown in Fig. 5(a). Interestingly, magnetic ferrites can also be used for $NaBH_4$ hydrolysis for H_2 generation, as well as Co and Ni nanoparticles. Here, two types of magnetic metal nanoparticles ferrite and Co containing metal nanoparticles prepared within p(AMPS) cryogels were used for H_2 production from hydrolysis of $NaBH_4$. As illustrated in Fig. 5(b), the inherently magnetic field responsive behavior of a catalyst offers control over the reaction system by an externally applied magnetic field. The preparation of ferrite metal

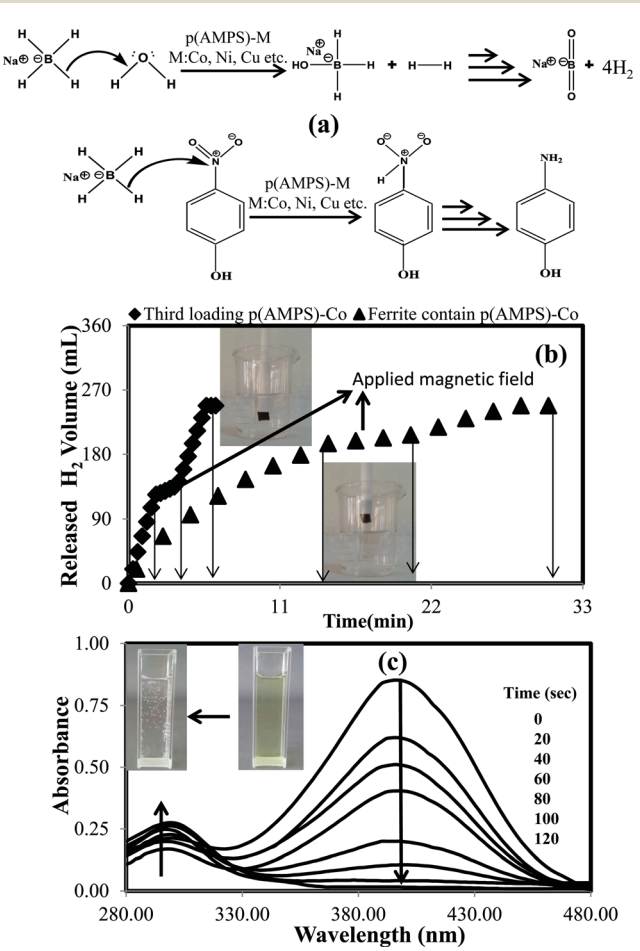

Fig. 5 (a) Reaction mechanisms for H_2 generation from hydrolysis of $NaBH_4$, and reduction of 4-NP. (b) H_2 generation from hydrolysis of $NaBH_4$ *via* ferrite-containing 0.1 g p(AMPS)–Co metal nanoparticles (8.71 mg nanoparticles) and magnetic three times Co(II) loaded-reduced 0.1 g p(AMPS)–Co (19.54 mg g^{-1} nanoparticles) catalyst system under an externally applied magnetic field. [Reaction conditions: 50 mL of 50 mM $NaBH_4$, 5 wt% NaOH, 30 °C, mixing rate of 1000 rpm.] (c) UV-Vis spectra of 4-NP reduction to 4-AP obtained using 0.1 g of p(AMPS)–Co cryogel composite catalyst systems (8.62 mg of Co nanoparticles). [Reaction conditions: 50 mL of 0.01 M 4-NP, 0.28 M $NaBH_4$, 30 °C, mixing rate of 1000 rpm].

nanoparticles was done according to the literature,[16] briefly, 0.1 g of p(AMPS) cryogels were immersed within a metal ion solution containing a 1 : 2 mole ratio of Fe(II) (0.05 M) : Fe(III) (0.1 M) mixture in 100 mL of aqueous solution for 12 h. Then, these iron ion-loaded cryogels were washed for 1 h to remove unbound metal ions from the cryogel matrices, and then placed in 100 mL of 0.5 M sodium hydroxide solution for 5 h to convert the iron ions into ferrite magnetic particles. Additionally, magnetic p(AMPS) cryogels were also prepared with Co(II) ions after three loading and reduction cycles as mentioned in Section 2.3. After the first loading and reduction of Co(II) ions into p(AMPS) cryogels, the prepared p(AMPS)–Co composites were placed again in 500 mL of 500 ppm Co(II) ion solution for 5 h, and then reduced to metal nanoparticles with 50 mL of 50 mM $NaBH_4$ solution for 3 h treatment, and the same procedure was repeated three times to increase the Co metal nanoparticle content of p(AMPS) cryogel with magnetic field responsive behavior. The use of magnetic metal nanoparticles is very important to control the reaction *e.g.*, the catalyst systems can be removed from the reaction mixture and placed back into the reaction medium to control the catalytic reactions. As illustrated in Fig. 5(b), H_2 generation from the hydrolysis of $NaBH_4$ using 0.1 g of ferrite-containing p(AMPS)–Co (containing 8.71 mg Co nanoparticles) was stopped at 12.5 min by removing the catalyst system from the reaction medium, and continued at 22.5 min by placing it back into the reaction medium. The reaction conditions throughout this investigation were 50 mL of 50 mM $NaBH_4$, 5 wt% NaOH, 30 °C, and a mixing rate of 1000 rpm . The same H_2 production control was done by using a 3rd time Co(II) loaded and reduced p(AMPS)–Co composite cryogel catalyst system (containing 19.54 mg Co nanoparticles) at 2 and 4 min under the same conditions. The hydrolysis reaction was completed within 30 min with a ferrite-containing p(AMPS)–Co metal composite catalyst system whereas the hydrolysis reaction was completed in only 6 min with a three times-loaded p(AMPS)–Co cryogel composite catalyst system. Therefore, the inherently magnetic field responsive p(AMPS)–Co cryogel catalyst system provides a great advantage in controllable fast catalysis for energy applications. Moreover, the environmental application of the p(AMPS) cryogel catalyst system was demonstrated by using 0.1 g of p(AMPS)–Co metal composite for the reduction of 4-NP to 4-AP as illustrated in Fig. 5(c). The reduction of 4-NP was carried out using 50 mL of 0.01 M 4-NP by using first time Co(II) loaded and reduced p(AMPS)–Co cryogel composite catalyst system (containing 8.62 mg nanoparticles) in the presence of 50 mL of 0.28 M $NaBH_4$ at 30 °C and a mixing rate of 1000 rpm. The reduction of 4-NP was completed within 120 s by cryogel-based p(AMPS)–Co metal composites. This time is relatively fast in comparison to the reported values in the literature,[13,16,36,40–44] suggesting that the cryogel-based catalyst composite systems have great advantages for faster catalytic performances. When considering these results and comparing with papers reported in the literature, the highly porous, large and open interconnected structures of the cryogels provide great benefits in terms of fast reaction kinetics.[16,40–44] Therefore, the choice of superporous cryogels as the catalyst support, and the reaction media for catalytic applications is pertinent.

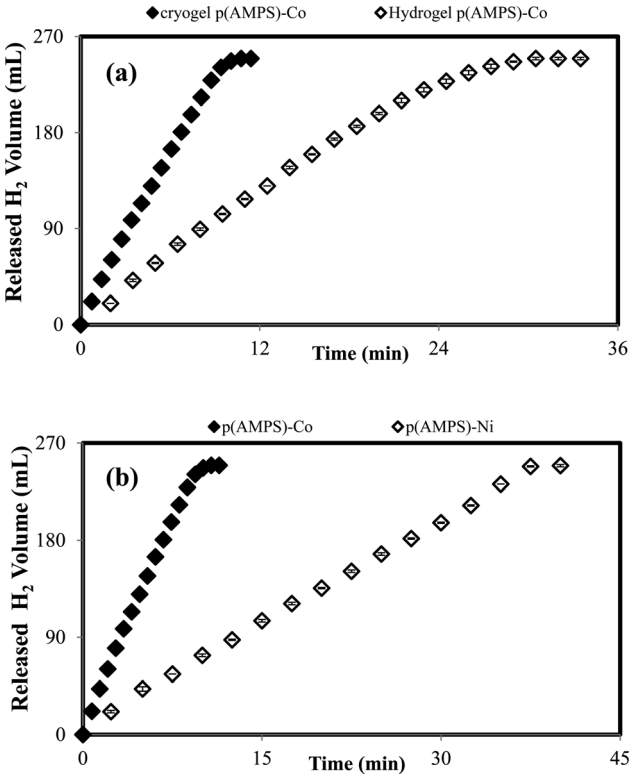

Fig. 6 (a) H_2 generation from hydrolysis of 50 mL of 50 mM $NaBH_4$ *via* 8.62 mg of Co nanoparticle-containing 0.1 g of cryogel p(AMPS)–Co composite, and 0.069 g of hydrogel p(AMPS)–Co composite. [Reaction conditions: 50 mL of 50 mM $NaBH_4$, 5 wt% NaOH, 30 °C, 1000 rpm.] (b) H_2 generation from hydrolysis of $NaBH_4$ *via* 0.1 g cryogel p(AMPS)–Co (8.62 mg Co nanoparticles) and 0.1 g p(AMPS)–Ni composites (8.94 mg Ni nanoparticles). [Reaction conditions: 50 mL 50 mM $NaBH_4$, 5 wt% NaOH, 30 °C, mixing rate of 1000 rpm].

3.3. The effect of porosity and metal types on $NaBH_4$ hydrolysis

To determine the effect of porosity, the H_2 production rates of conventional hydrogel and superporous cryogel p(AMPS)–Co composites were compared under the same reaction conditions; for example, 0.1 g of cryogel p(AMPS)–Co composite (containing 8.62 mg of nanoparticles) and 0.069 g of hydrogel p(AMPS)–Co composite (containing 8.62 mg of nanoparticles) were used for the hydrolysis of 50 mL of 50 mM $NaBH_4$, 5 wt% NaOH content, at 30 °C, and a mixing rate of 1000 rpm. The same amount (nearly 250 mL) of hydrogen was produced from the hydrolysis reactions and the reaction was completed within about 10 min using cryogel p(AMPS)–Co composite. The same reaction was completed within 30 min *via* the hydrogel p(AMPS)–Co composite as illustrated in Fig. 6(a). The H_2 production rate of the cryogel p(AMPS)–Co composite is three times faster than that of conventional hydrogel-supported metal composites. At the same time, as shown in Table 1, the Hydrogen Generation Rate (HGR), and Total Turnover Frequency (TOF) value of hydrogel p(AMPS)–Co composites were calculated as about 950 mL of H_2 per min per g

of metal and 2.24 mol H_2 per mol catalyst per min, whereas the HGR and TOF values of cryogel p(AMPS)–Co composites were calculated as 2697 mL of H_2 per min per g of M and 6.37 mol H_2 per mol catalyst per min, respectively. These values are 2.839 times and 2.844 times higher for the cryogel catalyst system, confirming the great benefit of porosity. The porosity of the cryogels enables easy and fast diffusion of the reactants and products in and out of the cryogel matrices and other species enabling faster kinetics with embedded metal nanoparticles inside the pores. This phenomenon is the main reason for the catalytic activity of the porous catalysts or cryogels and the most prominent distinct feature of the catalyst.

Different metal nanoparticles were prepared within cryogel matrices, and their catalytic performances were compared for the hydrolysis of $NaBH_4$ under the same reaction conditions as shown in Fig. 6(b). As can be seen, H_2 generation from the hydrolysis of $NaBH_4$ was completed in about 10 min by using 0.1 g of p(AMPS)–Co composite (containing 8.62 mg nanoparticles) whereas the same reaction was completed in about 40 min using the p(AMPS)–Ni composite (containing 8.94 mg of nanoparticles) under the same reaction conditions. The HGR of the cryogel p(AMPS)–Co and p(AMPS)–Ni composites were calculated to be 2700 and 700 mL H_2 per min per g of metal as given in Table 1. It is obvious that the HGR of the Co nanoparticle-containing p(AMPS) cryogels was nearly four-fold faster

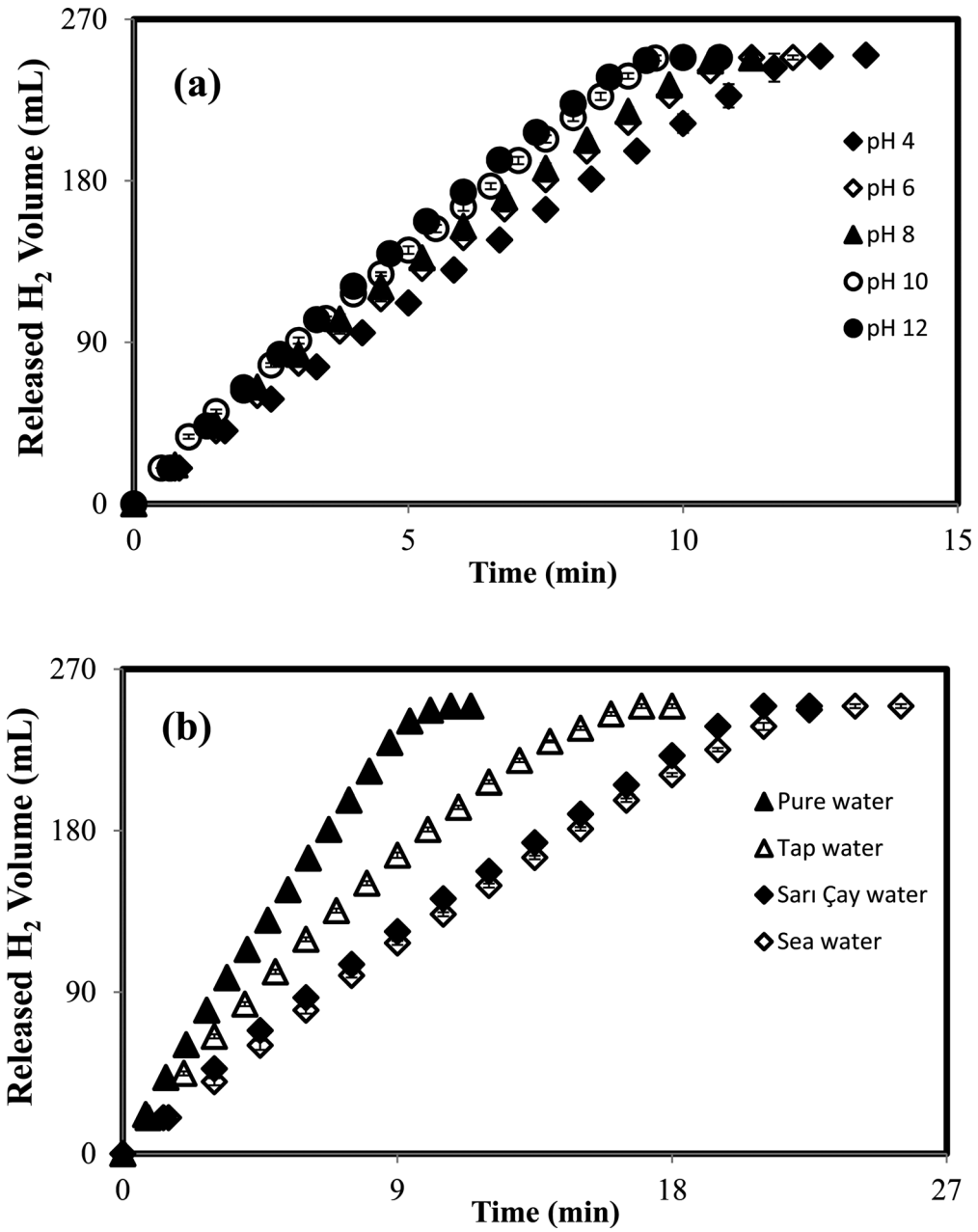

Fig. 7 (a) The effect of pH and (b) the effect of water type on H_2 generation reaction from hydrolysis of sodium borohydride *via* 0.1 g of cryogel p(AMPS)–Co (8.62 mg of nanoparticles). [Reaction conditions: 50 mL 50 mM $NaBH_4$, 5 wt% NaOH, 30 °C, mixing rate of 1000 rpm].

than that of the Ni nanoparticle-containing p(AMPS) cryogels, as expected since the Co nanoparticle catalytic performance is better than that of Ni nanoparticles in accordance with the literature.[16,17,37–44]

3.4. The effect of pH of the reaction medium and type of water on $NaBH_4$ hydrolysis

To determine the effect of pH of the medium on the hydrolysis reaction of $NaBH_4$ employing 0.1 g of p(AMPS)–Co metal composite (containing 8.62 mg of nanoparticles), five different pH values were tested *i.e.*, 4, 6, 8, 10 and 12 under the same reaction conditions as shown in Fig. 7(a). To adjust the pH of the reaction medium, 1 M HCl or 1 M NaOH were added into the hydrolysis medium and the obtained solutions with different pHs were used for the hydrolysis reaction of $NaBH_4$. Although the amount of produced H_2 gas was not affected by the change of medium pH, they all produced about 250 mL of H_2, the HGR of p(AMPS)–Co composites were affected as can be seen from the slope of Fig. 7(a). As can clearly be seen, as the pH of the $NaBH_4$ solution increased, the HGR also increased. The fastest hydrolysis reaction occurred at pH 12, and it reduced with decreasing pH values. In other words, the H_2 generation reaction of $NaBH_4$ was completed in about 10 min at pH 12, whereas the same reaction was completed in about 13 min at pH 4. Furthermore, the HGR and TOF values of the p(AMPS)–Co composite systems were calculated for different pHs and it was found that they both increased as the pH increased as given in Table 2. As the $NABH_4$ hydrolysis is generally performed in basic media these results comply with the literature.[16,40–44]

The hydrolysis reaction of $NaBH_4$ was also performed in four different types of water: pure water, tap water, Sarı Çay (local creek) water, and seawater, *via* the use of 0.1 g of p(AMPS)–Co composites (containing 8.62 mg nanoparticles) at the prescribed reaction conditions. As can be seen from Fig. 7(b), the HGR of the p(AMPS)–Co composites were strongly affected by the type of reaction water source. The fastest hydrolysis reaction, or highest HGR, was obtained in pure water whereas the slowest hydrolysis reaction, or the lowest HGR, was obtained in seawater. As can be seen from the figure, the H_2 generation reaction of $NaBH_4$ was completed within about 10 min in pure water, while the H_2 generation reaction of $NaBH_4$ was completed in about 25 min in seawater. The calculated HGR and TOF values were about 1288.99 ± 1.3 mL H_2 per min per g of M and 3.03 ± 0.5 mol H_2 per mol catalyst per min for seawater in comparison to 2697.91 ± 1 mL H_2 per min per g of M and 6.37 ± 0.4 mol H_2 per mol catalyst per min for DI water as illustrated in Table 2. As is very well known, the saltiness of sea water is higher than that of other types of water as compared with Sarı Çay water a creek water, tap water and DI water and this prevents higher TOF and HGR values from being obtained. In brief, due to the presence of different salts and some other impurities within seawater, creek waters and tap waters, the reduction in HGR and TOF valuables are plausible.

3.5. The effect of temperature on $NaBH_4$ hydrolysis

The effect of temperature on the hydrolysis of $NaBH_4$ was studied using 0.1 g of p(AMPS)–Co composites at different temperatures between 30 °C and 70 °C with 10 °C increments under the same reaction conditions: 50 mL of 50 mM $NaBH_4$ (containing 5 wt% NaOH), a mixing rate of 1000 rpm, using 0.1 g of p(AMPS)–Co (containing 8.62 mg g^{-1} Co). In addition, the hydrolysis reaction of $NaBH_4$ was investigated under relatively colder conditions *e.g.*, 0 °C. This process was carried out in a water-ice bath, and the temperature was kept constant by constantly adding ice around the reaction flask. As illustrated in Fig. 8(a), although the amount of hydrogen produced remained the same, 250 mL of H_2, for all the reaction temperatures, the time taken to produce the same amount of H_2 dramatically decreased with an increase in temperature. The hydrolysis reaction of $NaBH_4$ was completed in about 2 min at 70 °C, whereas it was completed in about 77 min at 0 °C, as shown in the inset of Fig. 8(a). The highest HGR and TOF values were obtained for the hydrolysis reaction that occurred at 70 °C as 14 501.16 ± 1 mL H_2 per min per g of m and 34.25 ± 1.2 mol H_2 per mol catalyst per min as given Table 2. As an increase in temperature increases the reaction rates, an increase of HGR and TOF values with an increase in the hydrolysis of $NaBH_4$ was expected.[40–44] The increase in reaction temperature leads to an increase in the reaction rates due to the increase in the number effective collisions with the reactants and catalyst. Therefore, the reaction rate of hydrogen generation increases with an increase in the reaction temperature. The kinetic parameters of the hydrolysis reaction of $NaBH_4$ were calculated by using the very-well known Arrhenius (eqn (4)) and Eyring (eqn (5))

Table 2 The change in TOF and HGR values of cryogel p(AMPS)–Co metal composites (8.62 mg of nanoparticles) depending on different reaction conditions[a]

Change in TOF and HGR values with temperature, pH, reuse and the types of reaction water											
T (°C)	TOF	HGR	pH	TOF	HGR	Reuse	TOF	HGR	Water	TOF	HGR
0 ± 2	0.89 ± 0.5	376.65 ± 1.2	4	5.47 ± 0.8	2320.18 ± 1.5	1st	6.37 ± 0.5	2697.91 ± 0.5	DI	6.37 ± 0.4	2697.91 ± 1
40 ± 1	11.74 ± 0.8	4974.66 ± 1	6	5.70 ± 1.2	2416.86 ± 1.2	2nd	6.32 ± 0.7	2677.96 ± 1.1	Tap	4.04 ± 0.7	1706.01 ± 1.2
50 ± 1	17.12 ± 1	7250.58 ± 1.5	8	6.08 ± 0.5	2577.98 ± 1	3rd	5.87 ± 0.5	2487.33 ± 1.6	Sarı Çay	3.26 ± 0.3	1381.06 ± 1.5
60 ± 1	24.90 ± 1	10 546.29 ± 1	10	6.22 ± 1	2636.57 ± 0.8	4th	5.47 ± 1	2320.18 ± 1.5	Sea	3.03 ± 0.5	1288.99 ± 1.3
70 ± 1	34.25 ± 1.2	14 501.16 ± 1	12	6.63 ± 0.6	2807.58 ± 1	5th	5.26 ± 1	2230.95 ± 1.2			

[a] TOF (Total Turnover Frequencies) [mol H_2 per mol catalyst per min]. HGR (Hydrogen Generation Rate) [mL H_2 per min per g of M].

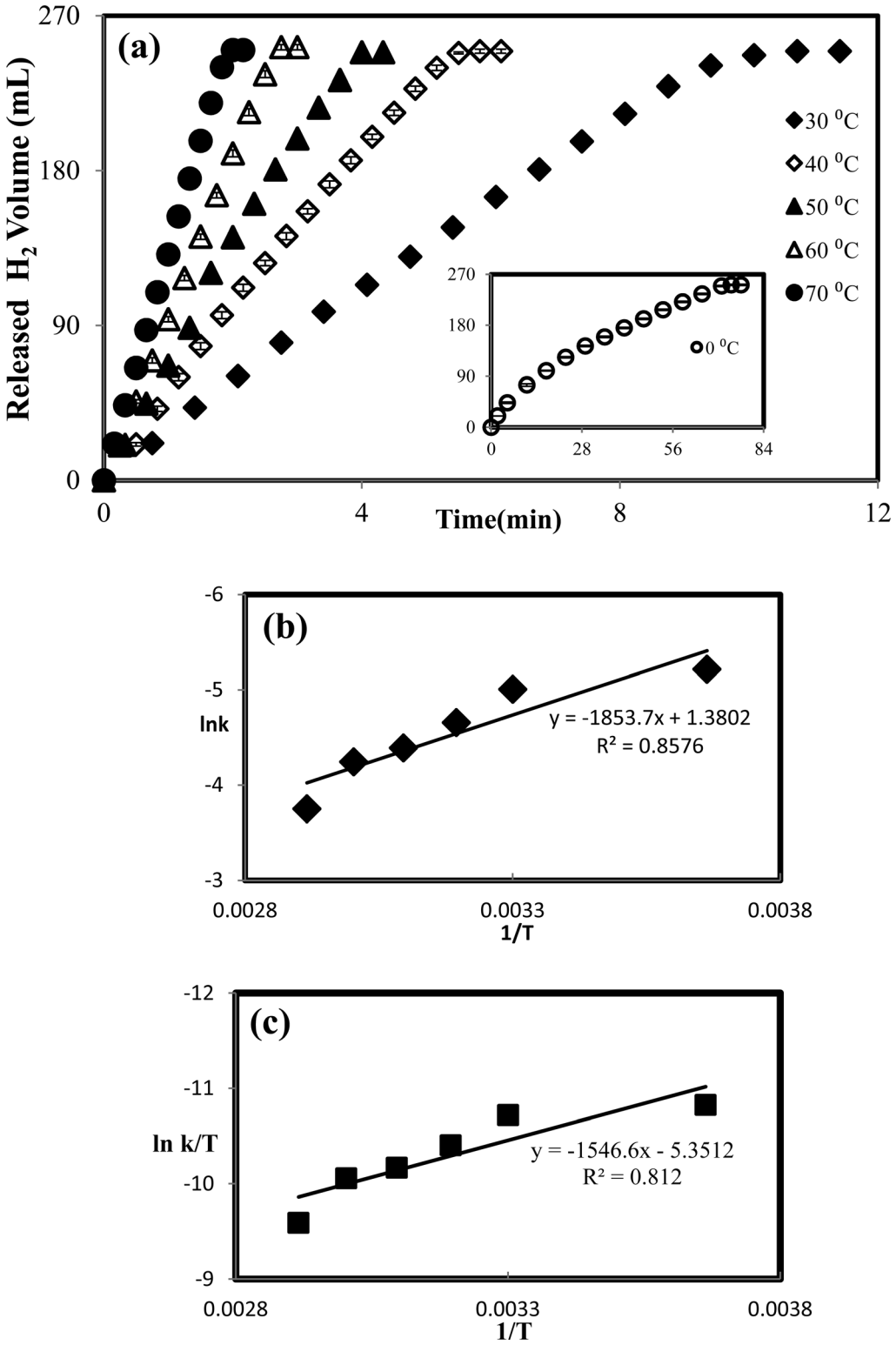

Fig. 8 (a) The effect of temperature on the hydrolysis of $NaBH_4$, (b), ln *k versus* 1/*T* (Arrhenius eqn.), and (c), ln(*k*/*T*) *versus* 1/*T* (Eyring eqn.). [Reaction conditions: 50 mL of 50 mM $NaBH_4$, 5 wt% NaOH, 1000 rpm, 8.62 mg of Co nanoparticles in 0.1 g of cryogel p(AMPS)–Co composite].

equations associated with the graphs ln *k versus* $1/T$ and $\ln(k/T)$ *versus* $1/T$ graphs.[38,39]

$$\ln k = \ln \mathrm{A} - (E_a/RT) \quad (4)$$

$$\ln(k/T) = \ln(k_B/h) + (\Delta S\#/R) - (\Delta H\#/R)(1/T) \quad (5)$$

Here, k is the reaction rate constant and was calculated according to a zero-order kinetic expression, E_a is the activation

energy, T is the absolute temperature, k_B is the Boltzmann constant (1.381×10^{-23} J K^{-1}), h is Planck's constant (6.626×10^{-34} J s^{-1}), ΔH is the activation enthalpy, ΔS is the entropy and R is the gas constant (8.314 J K^{-1} mol^{-1}). The kinetic parameters such as energy, enthalpy and entropy of cryogel p(AMPS)–Co composite systems were $E_a = 15.40 \pm 0.3$ kJ mol^{-1}, $\Delta H = 12.85 \pm 0.2$ kJ mol^{-1} and $\Delta S = -153.05 \pm 0.5$ J mol^{-1} K^{-1}, respectively. The activation energy values reported here for cryogel p(AMPS)–Co composite systems is one of the lowest in comparison to conventional hydrogels [16, 17 *etc.*]. This value proves that cryogel p(AMPS)–Co composite systems can be very useful for catalytic applications.

3.6. The reusability of p(AMPS)–Co macroporous composites

The reusability of the porous p(AMPS)–Co composite catalyst systems was investigated by using them consecutively in the same hydrolysis reaction. In brief, 0.1 g of cryogel p(AMPS)–Co composite (containing 8.62 mg nanoparticles) was used for H_2 generation from $NaBH_4$ hydrolysis under the usual reaction conditions (50 mL of 50 mM $NaBH_4$, 5 wt% NaOH content, at 30 °C and a mixing rate of 1000 rpm). After the first use, the p(AMPS)–Co metal composites were removed from the reaction medium, washed with plenty of water, and again placed into a similar fresh reaction medium under the same conditions and these steps were carried out five consecutive times. As illustrated in Fig. 9, there is no change in the conversion of $NaBH_4$ for H_2 generation but its activity was reduced from 100% to 82% at the end of the 5th use. The activity is calculated based on theinitial HGR to the HGRs of each use. The HGR and TOF values for the p(AMPS)–Co composite systems decreased to 2230 mL H_2 per min per g of M and 5.26 mol H_2 per mol catalyst per min from 2697 mL H_2 per min per g of M and 6.37 mol H_2 per mol catalyst per min, respectively, at the end of 5th use as can be seen in Table 2. The mass loss of catalyst during the catalytic reaction was not observed as the amounts of metal ions were determined before and after the hydrolysis reactions. However, due to the formation of $NaBO_2$ and its accumulation on the catalytic composite system, the activity decreased as we checked that there is no leakage or elution of metal nanoparticles from the cryo- and hydrogels networks.[16,40–44] The reduction in the catalytic performance of hydrogel–metal composites with repetitive use has been previously reported in the literature. For example, the reusability of p(VPA), p(AAm-co-VSA) and p(SPM) have been previously reported as being about 15, 55, and 72%, respectively.[18,43,44] Therefore, it can be said that although there is a reduction in the activity of cryogel p(AMPS)–Co composite, it can be used successively with 100% conversion for H_2 production from $NaBH_4$.

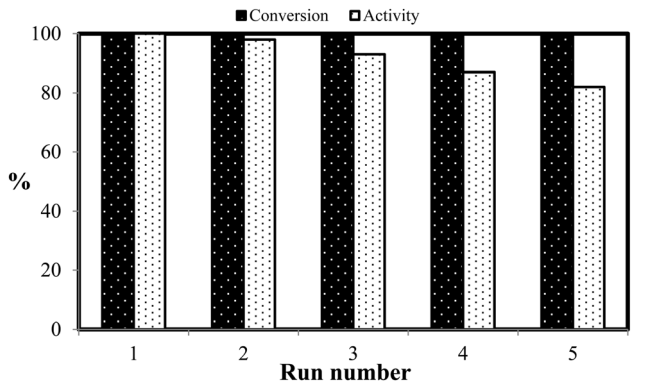

Fig. 9 The activity and the conversion ability of the cryogel p(AMPS)–Co composite for repetitive $NaBH_4$ hydrolysis. [Reaction conditions: 50 mL of 50 mM $NaBH_4$, 5 wt% NaOH, 30 °C, 1000 rpm, 8.62 mg of Co nanoparticles in 0.1 g of cryogel].

4. Conclusions

Due to the appealing properties such as the excellent chemical stability, improved response rates and diffusion of solutes, the super porous structure, and mechanical stability of cryogels, p(AMPS) cryogels were prepared and used as templates for the *in situ* metal nanoparticle preparation of Co and Ni and the resultant composites were used as catalyst media. Here, we have successfully demonstrated the use of macroporous cryogel p(AMPS)–Co composites in energy and environmental applications *via* H_2 generation from the hydrolysis of $NaBH_4$, and the reduction of toxic 4-NP to 4-AP, respectively.

The following conclusions and inferences can be deduced from this research:

- p(AMPS)-based superporous cryogels and conventional hydrogels were used for the metal nanoparticle preparation of Co and Ni, as catalysis media for 4-NP reduction and for H_2 generation from the hydrolysis of $NaBH_4$. It was found that Co nanoparticle-containing cryogel p(AMPS) provided better catalytic performances than its Ni nanoparticle-containing counterparts. The catalytic performances of Co-containing cryogel and conventional p(AMPS) hydrogel were compared for H_2 generation from the hydrolysis of $NaBH_4$ and the cryogel p(AMPS)–Co composite exhibited superior catalytic performance.
- Kinetic parameters such as energy, enthalpy and entropy of superporous cryogel p(AMPS)–Co composite systems for H_2 generation from the hydrolysis of $NaBH_4$ were calculated as $E_a = 15.40 \pm 0.3$ kJ mol^{-1}, $\Delta H = 12.85 \pm 0.2$ kJ mol^{-1} and $\Delta S = -153.05 \pm 0.5$ J mol^{-1} K^{-1}. This activation energy is one of the lowest E_a reported in the literature from similar studies.
- The superporous cryogel p(AMPS)–Co composite can also be used in various environmental applications such as nitro compound reduction and elimination of contamination by dyes, pesticides *etc.*
- Here, it can be summarized that cryogels with a superporous structure can be used in many applications due to their added properties compared to smart or intelligent hydrogels.

Acknowledgements

This work was supported by the Scientific and Technological Research Council of Turkey (113T042) and (110T649).

Notes and references

1 T. K. Zheleva and R. Ridolfi, *Energy*, 2006, **31**, 2486.
2 A. N. Ökte and D. Karamanis, *Appl. Catal., B*, 2013, **142–143**, 538.
3 D.-W. Zhuang, J.-J. Zhang, H.-B. Dai and P. Wang, *Int. J. Hydrogen Energy*, 2013, **38**, 10845.
4 T. P. Bartkus, J. S. Tiena and C.-J. Sung, *Int. J. Hydrogen Energy*, 2013, **38**, 4024.
5 H. Li, J. Liao, X. Zhang, W. Liao, L. Wen, J. Yang, H. Wang and R. Wang, *J. Power Sources*, 2013, **239**, 277.
6 A. Sartbaeva, V. L. Kuznetsov, S. A. Wells and P. P. Edwards, *Energy Environ. Sci.*, 2008, **1**, 79.
7 J. Shen, Y. Zhang, X. Xu, C. Hua, X. Sun, J. Li, Y. Mu and L. Wang, *Water Res.*, 2013, **47**, 5511.
8 X.-K. Kong, Z.-Y. Sun, M. Chen, C.-L. Chen and Q.-W. Chen, *Energy Environ. Sci.*, 2013, **6**, 3260.
9 M. H. Loghmani and A. F. Shojaei, *J. Alloys Compd.*, 2013, **580**, 61.
10 Y. Guo, Q. Feng, Z. Dong and J. Ma, *J. Mol. Catal. A: Chem.*, 2013, **378**, 273.
11 A. Chinnappan, H.-C. Kang and H. Kim, *Energy*, 2011, **36**, 755.
12 H. Li, J. Liao, X. Zhang, W. Liao, L. Wen, J. Yang, H. Wang and R. Wang, *J. Power Sources*, 2013, **239**, 277.
13 N. Sahiner, H. Ozay, O. Ozay and N. Aktas, *Appl. Catal., B*, 2010, **101**, 137.
14 M. B. Romanello and M. M. Fidalgo de Cortalezzi, *Water Res.*, 2013, **47**, 3887.
15 M. D. W. Grogan, S. C. Heck, L. M. Xiao, R. England, S. A. Maier and T. A. Birks, *J. Non-Cryst. Solids*, 2012, **358**, 241.
16 N. Sahiner, *Prog. Polym. Sci.*, 2013, **38**, 1329.
17 N. Sahiner and A. O. Yasar, *Fuel Process. Technol.*, 2013, **111**, 14.
18 N. Sahiner and S. Sagbas, *Colloids Surf., A*, 2013, **418**, 76.
19 S. Reichelt, A. Prager, C. Abe and W. Knolle, *Radiat. Phys. Chem.*, 2014, **94**, 40.
20 V. Stoyneva, D. Momekova, B. Kostova and P. Petrov, *Carbohydr. Polym.*, 2014, **99**, 825.
21 P. Karacan and O. Okay, *React. Funct. Polym.*, 2013, **73**, 442.
22 S. T. Koshy, T. C. Ferrante, S. A. Lewin and D. J. Mooney, *Biomaterials*, 2014, **35**, 2477.
23 B. Kostova, D. Momekova, P. Petrov, G. Momekov, N. Toncheva-Moncheva, C. B. Tsvetanov and N. Lambov, *Polymer*, 2011, **52**, 1217.
24 P. Petrova, A. Utrata-Wesołek, B. Trzebicka, C. B. Tsvetanova, A. Dworak, J. Aniol and A. Sieron, *Eur. Polym. J.*, 2011, **47**, 981.
25 S. Zheng, T. Wang, D. Liu, X. Liu, C. Wang and Z. Tong, *Polymer*, 2013, **54**, 1846.
26 K.-H. Chang, H.-T. Liao and J.-P. Chen, *Acta Biomater.*, 2013, **9**, 9012.
27 P. Petrov, E. Petrova, B. Tchorbanov and C. B. Tsvetanov, *Polymer*, 2007, **48**, 4943.
28 M. B. Dainiak, I. U. Allan, I. N. Savina, L. Cornelio, E. S. James, S. L. James, S. V. Mikhalovsky, H. Jungvid and I. Y. Galaev, *Biomaterials*, 2010, **31**, 67.
29 V. M. Gunkoa, V. V. Turov, V. I. Zarko, E. M. Pakhlov, G. P. Prykhodko, O. S. Remeza, R. Leboda, J. Skubiszewska-Ziebab and J. P. Blitz, *Colloids Surf., A*, 2013, **436**, 618.
30 V. I. Lozinsky, I. Y. Galaev, F. M. Plieva, I. N. Savina, H. Jungvid and B. Mattiasson, *Trends Biotechnol.*, 2003, **21**, 445.
31 M. M. Ozmen and O. Okay, *Polymer*, 2005, **46**, 8119.
32 B. Akduman, M. Uygun, D. A. Uygun, S. Akgöl and A. Denizli, *Mater. Sci. Eng., C*, 2013, **33**, 4842.
33 N. Bereli, D. Türkmen, K. Köse and A. Denizli, *Mater. Sci. Eng., C*, 2012, **32**, 2052.
34 K. Tekin, L. Uzun, C. A. Sahin, S. Bektas and A. Denizli, *React. Funct. Polym.*, 2011, **71**, 985.
35 N. Bereli, G. Sener, E. B. Altıntas, H. Yavuz and A. Denizli, *Mater. Sci. Eng., C*, 2010, **30**, 323.
36 L. Ai and J. Jiang, *Bioresour. Technol.*, 2013, **132**, 374.
37 J. C. Walter, A. Zurawski, D. Montgomery, M. Thornburg and S. Revankar, *J. Power Sources*, 2008, **179**, 335.
38 D. Xu, P. Dai, X. Liu, C. Cao and Q. Guo, *J. Power Sources*, 2008, **182**, 616.
39 A.-J. Hung, S.-F. Tsai, Y.-Y. Hsu, J.-R. Ku, Y.-H. Chen and C.-C. Yu, *Int. J. Hydrogen Energy*, 2008, **33**, 6205.
40 N. Sahiner, S. Butun and T. Turhan, *Chem. Eng. Sci.*, 2012, **82**, 114.
41 S. Sagbas and N. Sahiner, *Fuel Process. Technol.*, 2012, **104**, 31.
42 T. Turhan, Y. G. Avcibasi and N. Sahiner, *J. Ind. Eng. Chem.*, 2013, **19**, 1218.
43 F. Seven and N. Sahiner, *Int. J. Hydrogen Energy*, 2013, **38**, 777.
44 T. Turhan, T. G. Avcibasi and N. Sahiner, *Energy*, 2013, **55**, 511.